Quadrupolar Effect in X-Ray Magnetic Circular Dichroism

Christine Giorgetti and Elisabeth Dartyge
Laboratoire pour l'Utilisation du Rayonnement Electromagnétique, bâtiment 209D, F-91405 Orsay Cedex, France

Christian Brouder and François Baudelet
Laboratoire pour l'Utilisation du Rayonnement Electromanétique, bâtiment 209D, F-91405 Orsay Cedex, France and Laboratoire de Métallurgie Physique et Sciences des Matériaux, BP.239, F-54506 Nancy, France

Claire Meyer, Stefania Pizzini, Alain Fontaine, and Rose-Marie Galéra
Laboratoire de Magnétisme Louis Néel, 23 rue des Martyrs, B.P.166, F-38042 Grenoble Cedex 9, France
(Received 9 June 1995)

Quadrupolar ($E2$) transitions in x-ray magnetic circular dichroism at the L_{III} edge of Yb in $YbFe_2$ are evidenced through temperature and angular dependences. The choice of Yb is particularly relevant since $E2$ transitions come as a single peak. The width, position, and intensity of the $E2$ contribution are determined. The $E2$ peak appears in the middle of the dipolar signal. These measurements allow for the determination of dipole and octupole moments of the $4f$ shell, whose angular and temperature dependences were found to be in agreement with calculation.

PACS numbers: 78.70.Dm, 78.20.Ls

Interpretation of x-ray magnetic circular dichroism (XMCD) at the $L_{II,III}$ edges of rare earths is still a matter of discussion. Carra and Altarelli pointed out that electric quadrupolar ($E2$) transitions towards the $4f$ shell might be significant in these spectra [1]. They showed that this $E2$ contribution could be observed through its angular dependence which is different from the $\cos\theta$ variation of dipolar ($E1$) transitions (θ is the angle between the magnetic moment and the x-ray wave vector). Further calculations [2–7] and other spectroscopic techniques [8,9] confirmed the relevance of $E2$ transitions. After many unsuccessful experiments [10], the first evidence for $E2$ contributions to XMCD was published recently [11], confirming the idea that the low-energy peak is entirely due to $E2$ transitions [5]. On the contrary, we show that the $E2$ peak lies *between two E1 features* in $YbFe_2$.

$E2$ angular dependence can be written as [4,12–15]

$$\sigma(\theta) = A\cos\theta + B\cos\theta(5\cos^2\theta - 3), \qquad (1)$$

where A and B have different temperature dependences for rare earths. This point of view was confirmed by the change in shape observed in some rare-earth spectra [16].

In this paper, we study the $E2$ contributions to XMCD at the L_{III} edge of Yb in $YbFe_2$. Firstly, we show the angular dependence of XMCD at 10 K; secondly, we prove that the peak corresponding to $E2$ transitions exhibits the temperature dependence calculated from the crystal and exchange fields of the compound. These results enable us to characterize the position, width, and intensity of the $E2$ transitions and to compare them with the corresponding calculated quantities. The dipole and octupole moments of the $4f$ shell can be discriminated and measured with this technique.

The choice of Yb is particularly relevant to point out $E2$ transitions, since the $E2$ contribution to XMCD is made of only one line at the L_{III} edge and does not exist at the L_{II} edge. The initial and final state configurations can be written as $2p^6 4f^{13}$ and $2p^5 4f^{14}$, respectively. The ground state of Yb^{3+} is $J = 7/2$, and the possible final states are $J' = 1/2$ at the L_{II} edge and $J' = 3/2$ at the L_{III} edge. Because of the $E2$ selection rules ($|\Delta J| \leq 2$), only the $J' = 3/2$ final state can be reached. Since the $2p$ core hole is deep and the $2p$ spin-orbit is very large, no external perturbation (exchange or crystal field) can modify the LSJ coupling of the final states.

A more detailed analysis, using an expansion into elementary spectra [13] or the $E2$ sum rules [4], shows that the intensity of the $E2$ line for a powder is given by Eq. (1) for right-circularly polarized (negative helicity) x rays with $A = 30I^{(0)}\langle M\rangle$ and $B = I^{(0)}\langle \frac{185}{4} M - 5M^3\rangle$, where $\langle M\rangle$ and $\langle \frac{185}{4} M - 5M^3\rangle$ are the average value of $\langle J_z\rangle$ (dipole moment, proportional to the $4f$ magnetic moment) and $\langle [3J(J+1) - 1]J_z - 5J_z^3\rangle$ (octupole moment of the $4f$ shell) in the initial state (the z axis is along the $4f$ moment).

The advantage of Eq. (1) is that the geometrical factors ($\cos\theta$) and the details of the ground state ($\langle\cdots\rangle$) are decoupled so that temperature, magnetic field, or crystal field effects are summarized in the average values. $I^{(0)}$ is a positive number, proportional to the square of the reduced $E2$ matrix elements and to the number of holes [4,13]. According to Eq. (1), when the magnetic moment of Yb^{3+} is saturated ($M = -7/2$) and when the magnetic field and x-ray wave vector are aligned ($\theta = 0°$), the $E2$ contribution is zero. It becomes nonzero by rotating the magnetic field or raising the temperature, because the second term of Eq. (1) decreases faster with temperature

 0031-9007/95/75(17)/3186(4)$06.00

than the first term, which varies like the $4f$ magnetic moment. The great advantage of Yb is that the $E2$ contribution is a unique line. For other rare earths, a decomposition such as Eq. (1) is also possible, but $I^{(0)}$ is replaced by a spectral shape which is different for dipole and octupole moments [17].

The compound $YbFe_2$ crystallizes in the cubic Laves phase $MgCu_2$ structure at high pressure only. Previous magnetic and Mössbauer measurements have proved the trivalent state of Yb in $YbFe_2$ [18,19]. The present sample has been prepared in a Belt-type high pressure chamber [18], in the same conditions as in these former studies (8 GPa 1100 °C). The intermetallic alloy $YbFe_2$ has a Curie temperature $T_C = 543$ K. Yb is a heavy rare earth so the magnetic moments of Yb and Fe sublattices are antiparallel [20]. $YbFe_2$ has a compensation temperature T_{comp}, where each sublattice has equal net magnetic moment. The net magnetic moment of the Yb sublattice is larger than that of the Fe sublattice for $T < T_{comp}$ and smaller for $T > T_{comp}$. The compensation temperature $T_{comp} = 28 \pm 3$ K has been checked by measuring the thermal variation of the low field residual magnetization, after the saturation of the moments was achieved at room temperature under a 6 T magnetic field.

XMCD measurements at the L_{III} edge of Yb in $YbFe_2$ were carried out on the energy dispersive x-ray-absorption beam line of the positron-injected storage ring DCI at LURE, Orsay, France. The polychromator used was a curved Si(111) crystal, focusing between the poles of an electromagnet, where the sample was placed. Higher harmonics were rejected by a mirror positioned before a photodiode array detector. Right circularly polarized (helicity $-\hbar$) photons (polarization rate around 0.6) were selected by positioning a 1 mm wide slit 0.3 mrad below the synchrotron orbit plane.

The absorption spectra were measured on powder samples, in transmission geometry, in a magnetic field applied alternatively parallel (σ^+) and antiparallel (σ^-) to the propagation direction of the x-ray beam. To reach a good signal/noise ratio, the spectra are the average of 1900 pairs of measurements. The total data acquisition time was about 20 h. Low temperature measurements were done in a closed cycle refrigerator. The magnetic field on the sample was 0.34 T. The presented XMCD spectra are the difference ($\sigma^+ - \sigma^-$) divided by a constant value equal to the absorption edge step height. The origin of the energy scale was chosen as the steepest point in the raising edge (8944 eV for the L_{III} edge of Yb). Because of the compensation effect, the sign of XMCD spectra changes below and above T_{comp}.

Figure 1 presents the XMCD spectra measured at the L_{III} edge of Yb in $YbFe_2$ for angles θ equal to 0° and 66° at $T = 10$, 50, 100, 200, and 300 K. The angular dependence is expected to be maximum at low temperature. According to Eq. (1), the $E2$ peak should be negative for $\theta = 66°$ and zero for $\theta = 0°$ (at $T = 0$ K).

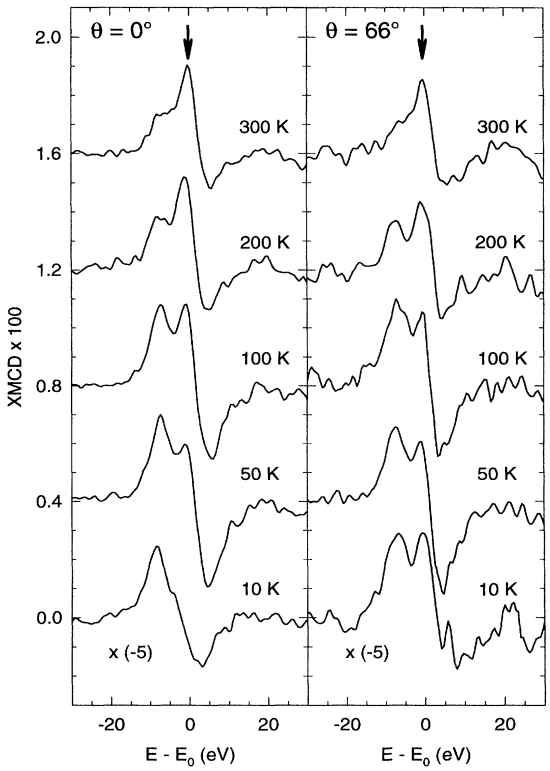

FIG. 1. Yb L_{III} edge XMCD spectra of $YbFe_2$ at $T = 10$ ($x - 5$), 50, 100, 200, and 300 K for 0° and 66°. Spectra for $\theta = 66°$ are divided by cos66°.

A comparison of the two spectra obtained at $T = 10$ K shows an additional peak around 0 eV for $\theta = 66°$, which is not visible for $\theta = 0°$. This peak is positive in Fig. 2 because the 10 K spectra have been reversed. The strong departure from the $\cos\theta$ dependence of the rest of the spectrum reveals unambiguously the $E2$ nature of the central peak.

The angular dependence yields one single $E2$ peak, as expected from theoretical arguments. At a temperature above T_{comp}, the spectra are reversed and are still made of three peaks. The $E2$ peak was extracted as the difference between the spectra at 100 and 50 K, suitably scaled to eliminate the $E1$ contribution. The resulting peak could be fitted with a Gaussian profile ($\sigma = 1.84$ eV, FWHM = 4.3 eV). Then, all spectra were analyzed as follows (see Fig. 2): (i) a straight line tangent to the XMCD signal (dotted line) was drawn between -5 and 4 eV, (ii) a Gaussian profile of width $\sigma = 1.84$ eV (full line) was fitted to the difference between XMCD and the straight line (dots), (iii) the so-called $E1$ spectrum (dashed line) was obtained as the difference between XMCD and the Gaussian fit. These $E1$ spectra are composed of two peaks of opposite sign, and they have a similar shape at all temperatures and angles.

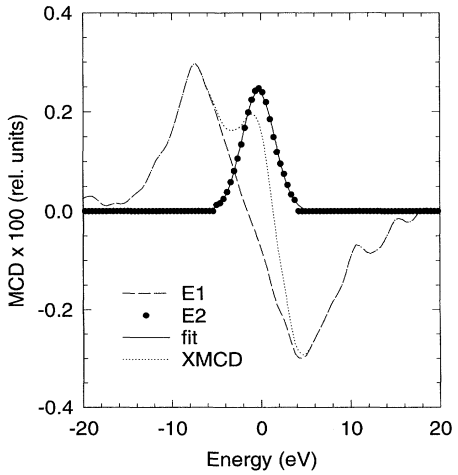

FIG. 2. Decomposition of the XMCD spectrum for 50 K and 0° (dotted line) as the sum of a Gaussian peak (full line) and an $E1$ contribution (dashed line). The dots result from the difference between the XMCD spectrum and a straight line drawn between -5 and 4 eV.

The temperature dependence of the intensities of $E1$ and $E2$ contributions is complex because the sample is not saturated and changes of magnetic moments are intermingled with anisotropy effects. Therefore we have studied the temperature dependence of the ratios (0° over 66°) of the $E1$ and $E2$ areas, which are presented in Fig. 3. As expected, the $E1$ ratios are consistent with a constant value of $1/\cos 66°$ (thin line). The $E2$ ratio starts from a very small value at 10 K and increases towards the $E1$ value at high temperature. We have simulated the $E2$ ratios by calculating $I(0°)/I(66°)$ from Eq. (1). The

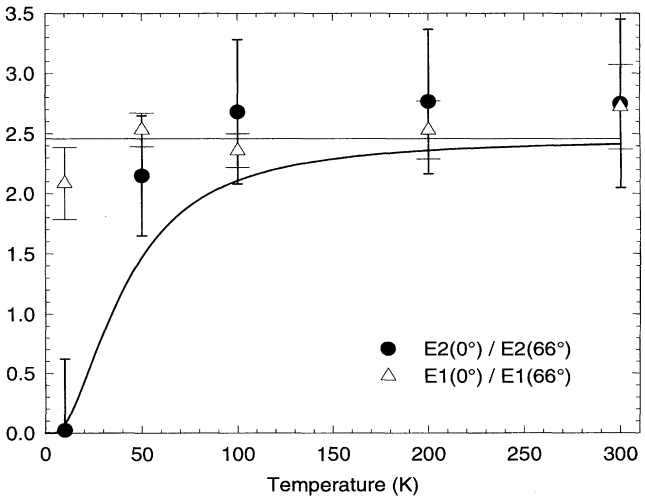

FIG. 3. Ratio of peak intensities of $\theta = 0°$ and 66° for $E1$ and $E2$ contributions. The thick (thin) full line is the calculated variation of the $E2$ ($E1$) contribution.

crystal field and exchange field parameters used for this calculation were taken from Ref. [19]. As seen in Fig. 3, the experimental variation is consistent with the calculated curve (thick full line), although the experimental points are somewhat above the computed values for $E2$. This discrepancy can be explained by noticing that, at 0.34 T, the magnetization is not saturated and the sample is a distribution of domains. This distribution can be taken into account by averaging over θ around a mean θ_0 in Eq. (1) [7].

From the width of the $E2$ peak, we calculated the absolute intensity of $E2$ transitions using Cowan's program [21], and we normalized them with respect to the edge jump using the absolute $E1$ cross sections published in Ref. [22]. The intensity of the $E2$ peak obtained for a fully saturated Yb ion at 0 K ($M = -7/2$, $\mu_{4f} = 4\mu_B$) and a polarization rate of 1 is 52×10^{-3}. XMCD measurement for an applied magnetic field of 1 T at 300 K (where $\mu_{4f} = 0.63\mu_B$) yields an $E2$ peak with intensity 4×10^{-3}. This corresponds to an $E2$ intensity of 25×10^{-3} at 0 K. The agreement is correct when the circular polarization rate is taken into account.

The third important parameter is the energy position of the $E2$ transitions. The position of the $E2$ peak with respect to the $E1$ white line can be compared with a relativistic ΔSCF calculation carried out with Desclaux' program [23]. The difference between the $2p^5 4f^{14} 5d^2 6s^1$ and $2p^5 4f^{13} 5d^3 6s^1$ average configuration energies is -10 eV. This is larger than the experimental energy difference between the top of the white line and the $E2$ peak (-5 eV). This energy shift can be used as a reference for the calculation of $E2$ contribution for the other rare earths. It is compatible with the energy difference between dipole and quadrupole contributions found by Krisch *et al.* [24].

By studying the angular variation of XMCD given in Eq. (1), and by comparing with calculated $E2$ transitions shapes, one can determine the dipole and octupole moments of the $4f$ shell. This is possible because the calculation of $E2$ transitions can be made accurately with atomic structure programs [21] and because all spectra can be written as the sum of a dipole and octupole moments multiplied by a fixed spectral shape [17]. The octupole part of the $E2$ transition can be obtained from angular dependent measurement. This allows for the determination of the position and width of $E2$ transitions. From these parameters we can calculate the dipole moment part [A in Eq. (1)] and extract it from the experimental spectra. The quadrupole moment can be determined for certain rare earths with Mössbauer spectroscopy. XMCD is a unique tool for the measurement of the octupole moment which can be used to fit the crystal and exchange field parameters of the compound.

The accurate determination of the quadrupole contribution is necessary to obtain a reliable $E1$ XMCD spectrum. At the L_{III} edge of Yb in $YbFe_2$ the $E1$ contribution to XMCD spectra is made of two peaks. A similar shape

was observed at the L_{III} edge of the heavy rare earths (R) in RFe_2 compounds [25]. This contradicts the idea that the first peak is due to $E2$ transitions [5]. In XMCD spectra at the L_{II} edge of Yb [26], only one peak is observed, so that the statistical ratio of -2 between $E1$ XMCD signals at the L_{II} and L_{III} edges is not satisfied. This is connected to the spin-orbit effect on the $5d$ shell.

In conclusion, the $E2$ transitions in XMCD were observed at the L_{III} edge of Yb in $YbFe_2$. Our results confirm unambiguously the prediction of Carra and Altarelli [1]. We have extracted the width, intensity, and energy position of these transitions and compared them with calculated values. Temperature variations of the ratios of $E2$ terms at 0° and 66° were found to agree with calculations. Dipole and octupole moments of the $4f$ shell can be determined from $E2$ spectra. This opens the way to an accurate determination of the $E1$ contribution and to the study of $5d$ magnetism in rare earths.

We are grateful to M. Perroux who prepared the sample in the high pressure setup of the Laboratoire de Cristallographie (CNRS, Grenoble) and thank Ph. Sainctavit, H. Maruyama, and J. Lang for their comments and suggestions.

[1] P. Carra and M. Altarelli, Phys. Rev. Lett. **64**, 1286 (1990).
[2] P. Carra *et al.*, Phys. Rev. Lett. **66**, 2495 (1991).
[3] J. C. Lang *et al.*, Phys. Rev. B **46**, 5298 (1992).
[4] P. Carra *et al.*, Physica (Amsterdam) **192B**, 182 (1993).
[5] X. D. Wang *et al.*, Phys. Rev. B **47**, 9087 (1993).
[6] X. D. Wang *et al.*, J. Appl. Phys. **75**, 6366 (1994).
[7] J. C. Lang *et al.*, Phys. Rev. B **49**, 5993 (1994).
[8] J. P. Hannon *et al.*, Phys. Rev. Lett. **61**, 1245 (1988).
[9] K. Hämäläinen *et al.*, Phys. Rev. Lett. **67**, 2850 (1991).
[10] $Ho_3Fe_5O_{12}$ [14,15,27], Gd_2Co_{17} [28], Er_2Co_{17} [28], $Er_2Fe_{14}B$ [3], $HoFe_2$ [29,30], $DyFe_2$ [30], $ErFe_2$ [30,]YIG [15], and $YbFe_2$ [16].
[11] J. C. Lang *et al.*, Phys. Rev. Lett. **74**, 4935 (1995).
[12] Ch. Brouder, *X-ray Absorption Fine Structure* (Ellis Horwood, New York, 1991), pp. 106-108.
[13] Ch. Brouder, *Compte-rendu des Journées Grand-Est*, edited by J.-P. Kappler (University of Strasbourg, Strasbourg, 1994), p. 53-7.
[14] K. Shimomi *et al.*, Jpn. J. Appl. Phys. **32**, Suppl. 32-2, 314 (1993).
[15] H. Yamazaki *et al.*, Jpn. J. Appl. Phys. **32**, Suppl. 32-2, 317 (1993).
[16] Ch. Giorgetti *et al.*, Physica (Amsterdam) **208-209B**, 777 (1995).
[17] The general formula for quadrupole transitions at the $L_{II,III}$ edges of rare earths is [13]

$$\sigma^Q(\omega) = \pi^2\alpha\hbar\omega\,\frac{10}{3}\,k^2\sum_a(2a+1)\sum_{J'}(-1)^{J+J'}\begin{Bmatrix}2 & 2 & a\\ J & J & J'\end{Bmatrix}\times|\langle J'\|r^2C^{(2)}\|J\rangle|^2\delta(E_{J'}-E_i-\hbar\omega)\times\sqrt{\frac{(2J-a)!}{(2J+a+1)!}}\sum_\alpha\langle i|T^{(a)}_\alpha|i\rangle(-1)^\alpha S^{(a)}_{-\alpha}$$

where

$$S^{(a)}_{-\alpha} = \sum_{mm'}\begin{pmatrix}2 & a & 2\\ m & -\alpha & m'\end{pmatrix}\sum_{\lambda\lambda'\mu\mu'}\begin{pmatrix}1 & 1 & 2\\ \lambda & \mu & m\end{pmatrix}\begin{pmatrix}1 & 1 & 2\\ \lambda' & \mu' & m'\end{pmatrix}\times(-1)^a\times C^{(1)}_\lambda(\hat{\boldsymbol{\epsilon}})C^{(1)}_\mu(\hat{\mathbf{k}})C^{(1)}_{\lambda'}(\hat{\boldsymbol{\epsilon}}^*)C^{(1)}_{\mu'}(\hat{\mathbf{k}}).$$

This equation describes the quadrupole contribution to XAFS as a sum of spectral shapes weighted by ground state properties of the $4f$ shell ($\langle i|T^{(a)}_\alpha|i\rangle$) [31], and by the polarization state of the x rays ($S^{(a)}_{-\alpha}$). For powders, the relevant terms are $S^{(0)}_0 = 1/(10\sqrt{5})$ and $T^{(0)}_0 = 1$ for the isotropic spectrum and

$$S^{(1)}_0 = \frac{i(\hat{\boldsymbol{\epsilon}}\times\hat{\boldsymbol{\epsilon}}^*)_z}{10\sqrt{30}} \quad\text{and}\quad S^{(3)}_0 = -\frac{i(\hat{\boldsymbol{\epsilon}}\times\hat{\boldsymbol{\epsilon}}^*)_z(5k_z^2-3)}{10\sqrt{70}}$$

$$T^{(1)}_0 = 2J_z \quad\text{and}\quad T^{(3)}_0 = 4[5J_z^2 - 3J(J+1)+1]J_z$$

for the MCD spectrum.
[18] C. Meyer *et al.*, J. Phys. **38**, 1449 (1977).
[19] C. Meyer *et al.*, J. Phys. **40**, 403 (1979).
[20] J. J. M. Franse and R. J. Radwański, in *Handbook of Magnetic Materials*, edited by K. H. J. Buschow (Elsevier, New York, 1993), Vol. 7.
[21] R. D. Cowan, *The Theory of Atomic Structure and Spectra* (University of California Press, Berkeley, 1981).
[22] E. B. Saloman *et al.*, At. Data Nucl. Data Tables **38**, 1 (1988).
[23] J. Desclaux, Comput. Phys. Commun. **9**, 31 (1975).
[24] M. H. Krisch *et al.*, Phys. Rev. Lett. **74**, 4931 (1995).
[25] Ch. Giorgetti, Ph.D. thesis, University of Orsay, 1994.
[26] Ch. Giorgetti *et al.* (unpublished).
[27] P. Fischer *et al.*, Solid State Commun. **82**, 857 (1992).
[28] P. Fischer *et al.*, J. Appl. Phys. **69**, 6144 (1991).
[29] F. Baudelet *et al.*, J. Electron. Spectrosc. Relat. Phenom. **62**, 153 (1993).
[30] J. C. Lang *et al.*, Phys. Rev. B **50**, 13 805 (1994).
[31] L. C. Biedenharn and J. D. Louck, *Angular Momentum in Qunatum Physics* (Addison-Wesley, London, 1981).